

CYCLIC SETTLEMENT AND SLIDING OF CAISSON SEAWALLS

Doug P STEWART¹, Randolph R SETTGAST², Bruce L KUTTER³, Tadashi KAWAI⁴, Shunichi HIGUCHI⁵ And Tomoyoshi TAKEDA⁶

SUMMARY

Man-made islands have recently been considered as possible new construction sites for a variety of facilities. The performance of seawalls bounding these islands when subject to seismic loading is an important aspect of design. To obtain data on the performance of such structures when founded on a loose sand seabed, a series of ten large scale centrifuge models were tested on the 9 m radius centrifuge at the University of California, Davis.

The models were each subject to a series of model earthquake base motions including sinusoidal and realistically scaled earthquake time histories. As expected, the concrete caissons were found to settle, displace laterally, and rotate away from the backfill. The experiments were designed to investigate the influence of the thickness and density of the sand seabed on the permanent deformations of the caisson walls, and test data is presented to illustrate these effects.

Due to the large amount of instrumentation in the model tests, it was possible to integrate and differentiate accelerometer data to obtain estimates of the dynamic "shear stress", "shear strain", and pore pressure in the loose sand beneath the caisson and settlement time histories for the caisson. These results are cross-plotted to produce approximate "stress"- "strain" curves, plots of "shear stress" as a function of "effective vertical stress", and "vertical strain" as a function of "shear strain". The plots show illuminating inter-relationships between these parameters and bear fascinating resemblance to data from conventional laboratory cyclic undrained simple shear tests.

INTRODUCTION

Recently in Japan, man-made islands have been considered as construction sites for a variety of facilities including airports and electric power generating facilities. Apart from the performance of the facility itself, one of the most important design issues when assessing the feasibility of this type of construction is the seismic performance of the seawalls bounding the island. As illustrated in Figure 1, a seawall structure will include segmental concrete caissons upon a crushed rock mound on the seabed surface. Crushed rock backfill and ballast is placed behind and within the caissons before installation of a concrete superstructure. The wall is protected on the seaward side by an armored embankment, possibly comprised of interlocking concrete armor units to dissipate wave energy and increase the stability of the wall. At potential sites being considered for such facilities near the Japanese coast, the seabed is comprised of sand of variable thickness underlain by rock.

Issues that need to be addressed during the design of this type of structure include the overall stability of the seawall and the deformations due to an earthquake. The seismic response of a structure similar to that depicted in Figure 1 is difficult to assess analytically. Little information about field performance of such structures is

¹ University of Western Australia, AUSTRALIA, stewart@civil.uwa.edu.au

² University of California, Davis, USA, rrsettgast@ucdavis.edu

³ University of California, Davis, USA, blkutter@ucdavis.edu

⁴ Central Research Institute of Electric Power Industry, JAPAN, t-kawai@criepi.denken.or.jp

⁵ Obayashi Corporation, JAPAN, higuchis@tri.obayashi.co.jp

⁶ Tokyo Electric Power Company, JAPAN, t0743799@pmail.tepco.co.jp

available, despite extensive data collected on the seismic performance of caisson type quay walls in the Kobe area (Inagaki et al., 1996). Therefore, to examine the behavior of this type of structure during an earthquake, a series of large centrifuge model tests was carried out. This paper describes the general response of the seawall models during strong ground motion events and presents summary data to illustrate the effect of thickness and density of the sand seabed substratum. Some results from these model tests were reported briefly by Kawai et. al (1998). An in-depth case history of one of the model tests is described by Stewart et al. (2000), along with a detailed description of the modeling techniques and an appraisal of the limitations of the work.

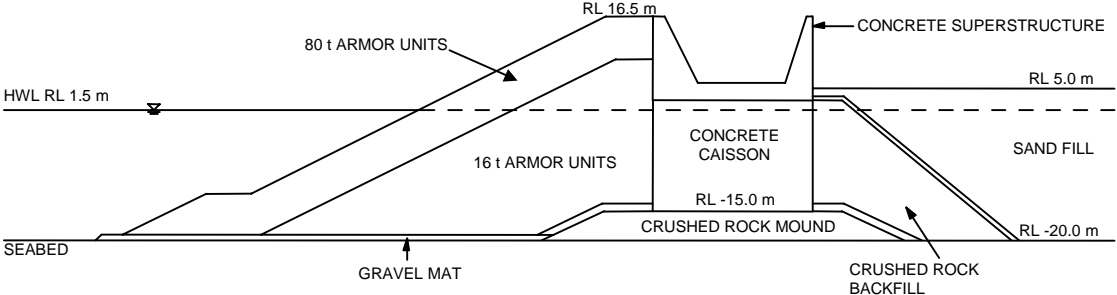


Figure 1. Prototype seawall for this study

EXPERIMENTAL EQUIPMENT AND PROCEDURES

To correctly represent in situ stresses and thus allow accurate simulation of soil behavior, the experiments were conducted on the large geotechnical centrifuge at the University of California, Davis. This centrifuge, in terms of radius (9.1 m to bucket floor), maximum payload mass (4500 kg), and available bucket area (4.0 m²) is currently one of the largest geotechnical centrifuges in the world. The shaker consists of two pairs of large single acting servo-hydraulic actuators having a peak dynamic driving capacity of 400 kN each. In practice, base shaking accelerations of up to 30 g have been generated. A detailed description of the shaker is given by Kutter et al. (1994). The principles of centrifuge modeling and scaling relationships are described in general by Schofield (1980), and as specifically relating to dynamic problems by Kutter (1995), and so will not be discussed here.

A rigid container was used in this study. In many dynamic tests it is desirable to use a container having flexible walls, so that the soil is able to deform in the correct manner and that boundary effects are minimized. However, a flexible container similar to those described by Fiegel et al. (1994) and Zeng and Schofield (1996) was unsuitable for the tests described here since the model geometry was not symmetrical, and would cause distortion of the container. The internal dimensions of the container are 1760 × 905 × 500 mm (length × width × height), with shaking in the direction of the length. The container has polycarbonate side walls to permit viewing of a cross section during testing.

The models tested in this study were based on the prototype seawall illustrated in Figure 1. Due to the large size of the prototype seawall, the size of the resulting centrifuge model would have exceeded the limits of the available facilities. Therefore, a simplified ¼ scale prototype seawall was modeled using a 1/30 scale centrifuge model. A typical centrifuge model is illustrated in Figure 2. Thus the centrifuge models in this study were actually 1/120 scale models of the full scale prototype seawall. All data presented in this paper are done so in terms of the ¼ scale prototype and no attempt is made to then scale the results to the full scale prototype.

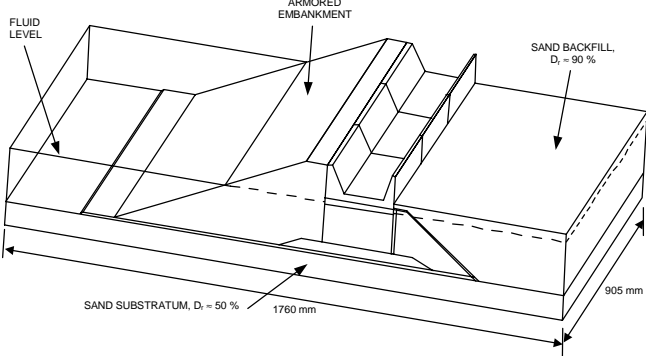


Figure 2. Layout of typical centrifuge model.

Following two preliminary tests, a total of ten models (denoted SW03 to SW12) were tested for this study. The "standard" model configuration (test SW05) illustrated in Figure 2 comprised a medium dense sand substratum ($D_r \approx 50\%$) of 2.5 m thickness at $\frac{1}{4}$ prototype scale (83 mm at model scale). In the "standard" model, the sand backfill was placed at a relative density of about 90 % or greater. The testing program covered the following variables: (a) density of the substratum between about 50 and 90 %, (b) thickness of the substratum between 1.25 and 5 m, (c) lateral extent of a region of higher density in the substratum (an improved zone), and (d) density of the sand backfill between about 60 and 90 %. In three tests (SW08 to SW10), a zone of soil beneath the caisson and armored embankment was prepared at a higher density ($D_r \approx 95\%$) than the remainder of the substratum ($D_r \approx 50\%$). The lateral extent of this denser region was varied and was intended to represent the effect of possible ground improvement works prior to construction of the seawall.

Table 1. Summary of model configurations.

Test	Description	Sand seabed		Sand fill
		thickness (m)	D_r (%)	D_r (%)
SW03	bearing directly on rock	0	-	84
SW04	uniform sand substratum	2.5	66	98
SW05	uniform sand substratum	2.5	54	93
SW06	uniform sand substratum	2.5	88	97
SW07	uniform sand substratum	1.25	54	90
SW08	improved below mound only (13.8 m width)	2.5	51/92	87
SW09	improved below mound + H (16.3 m width)	2.5	55/93	98
SW10	improved below mound and armored embankment (29.4 m width)	2.5	47/98	97
SW11	uniform sand substratum	2.5	53	61
SW12	uniform sand substratum	5	47	99

Nevada sand ($D_{10} = 0.10$ mm and $D_{50} = 0.17$ mm) was used to model the seabed and fill forming the island. The Nevada sand was found to have maximum and minimum dry densities of 1.71 and 1.42 Mg/m³ respectively ($e_{\min} = 0.55$ and $e_{\max} = 0.86$) by ASTM D4253-93 and ASTM D4254-91. A fine crushed rock ($D_{50} = 6.6$ mm), was used to construct the crushed rock mound and backfill shown in Figure 2. A coarse sand ($D_{50} = 1.6$ mm), was used for the gravel mat, a buffer zone adjacent to the caisson, and as part of a granular filter between the crushed stone backfill and the sand fill. The armored embankment was constructed from commercially supplied miniature concrete armor units. These were 1/120 scale representations of commercial 80 tonne Tetrapod units. Approximately 2500 individual armor units were used in each model. The concrete caisson and connected superstructure were formed in three segments that could be placed across the model container, Figure 2.

In order to model the time scaling for pore pressure generation and dissipation more correctly, a fluid having a viscosity ten times that of water was chosen as the pore fluid. A mixture of water and hydroxypropyl methylcellulose (HPMC), supplied under the trade name Methocel, was used as described by Stewart et al. (1998). The soil particle sizes and permeabilities in the field may be different to those of the Nevada Sand used in the models. The Nevada Sand and pore fluid viscosity used in the model represented soil in the $\frac{1}{4}$ scale prototype with a permeability of approximately 10^{-5} m/s.

About 64 instruments were included in each model. The instruments generally comprised about:

- 28 accelerometers placed within the sand layers and crushed rock mound, on the caisson and on the container base plate;
- 25 pore water pressure transducers placed within the sand layers, crushed rock mound and backfill, and against the caisson wall;
- 3 earth pressure transducers embedded in the rear face of the caisson; and
- 8 displacement transducers to measure settlement of the sand backfill surface and vertical and lateral movement of the caisson.

Each centrifuge model was initially subjected to a series of small base shaking events to assess the small strain dynamic response of the models without causing measurable deformation or generation of excess pore pressures. To test the response of the models under strong levels of shaking, a series of larger base shaking events were used. These events comprised 3 Hz fixed frequency sinusoidal motions, and a motion based upon a recording from RL -79 m at Port Island in Kobe, Japan during the 1995 Hyogo-Ken Nanbu earthquake.

GENERAL RESPONSE TO STRONG MOTIONS

The general model response during strong shaking was similar in all models tested. As an example of the time history data acquired from this series of experiments, selected time histories are presented in Figure 3 from the 0.5 g Kobe event from test SW12. The general response of the models can be summarized as follows:

- The caisson experienced settlement and lateral displacement (translation and rotation) away from the backfill. The majority of the displacements occurred during the shaking event, with small post-shaking settlements occurring due to pore pressure dissipation.
- The backfill experienced settlement due to densification, and lateral deformation away from the rigid end wall.
- The base accelerations were amplified up through the soil and seawall structure during the smaller events, as discussed by Kawai et al. (1998). During the larger events, there was a significant level of attenuation after the initial cycles of shaking.
- The pore water pressures in the sand strata exhibited a complex dynamic response, which was the result of a number of different phenomena. The substrata sands experienced a positive excess pore pressure buildup, as well as a high frequency cyclic response. The large high frequency negative spikes in pore pressure, which are consistent with dilatancy of the sand, are highly correlated to spikes in the caisson acceleration.

A more detailed description of the model response, and additional data, are presented by Stewart et al. (2000).

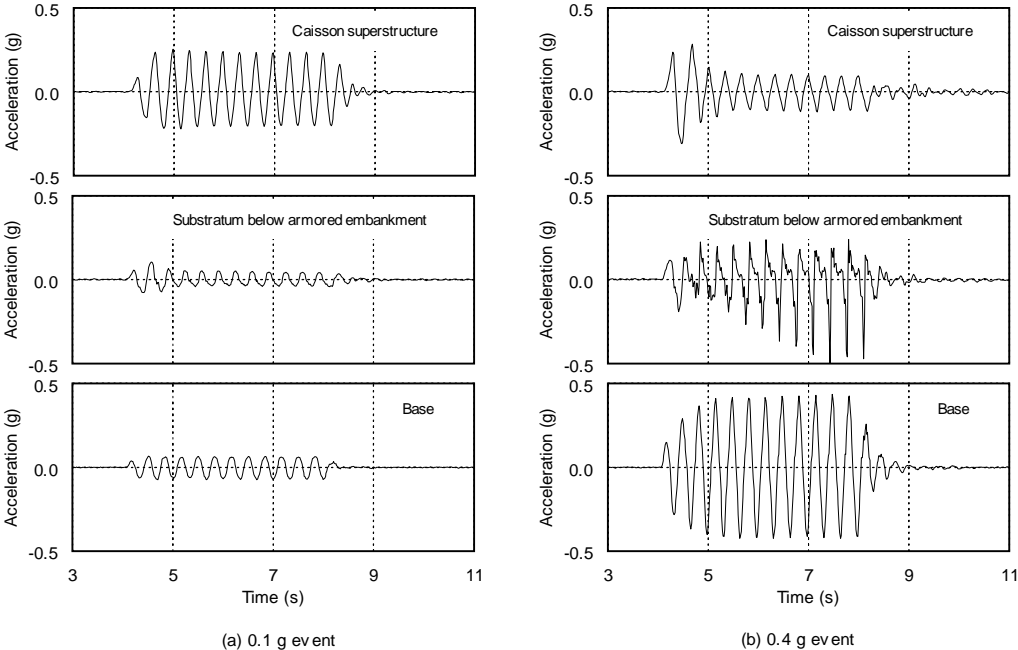


Figure 3. Selected acceleration time histories from 3 Hz events in SW12.

CAISSON DISPLACEMENT

Effect of Substratum Density

Figure 4 illustrates the effect of substratum density on displacement of the caisson, for tests where the substratum thickness was 2.5 m. Data from tests SW04, SW05, SW06 and SW11, where the substratum was of uniform, but different, density are shown. Settlement data from tests SW08, SW09 and SW10, where a region of

higher density was formed below the caisson, are also included in Figure 4(a) by using the relative density directly below the caisson. These data compare reasonably well with those from the tests with uniform density. The measured cumulative settlements are up to 7 % of the substratum thickness. However, the incremental settlements in each event are generally 1 to 2 % of the substratum thickness. As expected, an increase in density gives rise to lower settlement and lateral deformation. The data suggest there is a significant improvement in performance (especially lateral deformation) as the relative density increases from about 55 to 65 %. However, a detailed examination of other aspects of the test data suggested that the relative density may have been significantly higher than 66 % beneath the armored embankment in model SW04. Higher density in this region might be expected to inhibit lateral deformation more than vertical, and so it is likely that there should be a more gradual drop in lateral displacement than that shown in Figure 4(b).

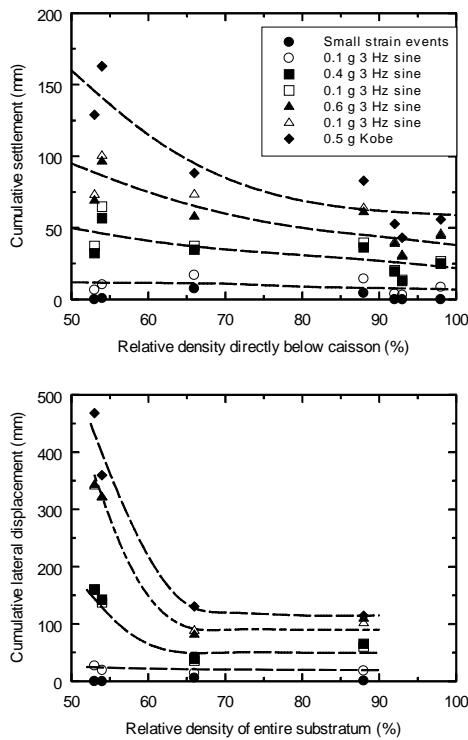


Figure 4. Effect of substratum density.

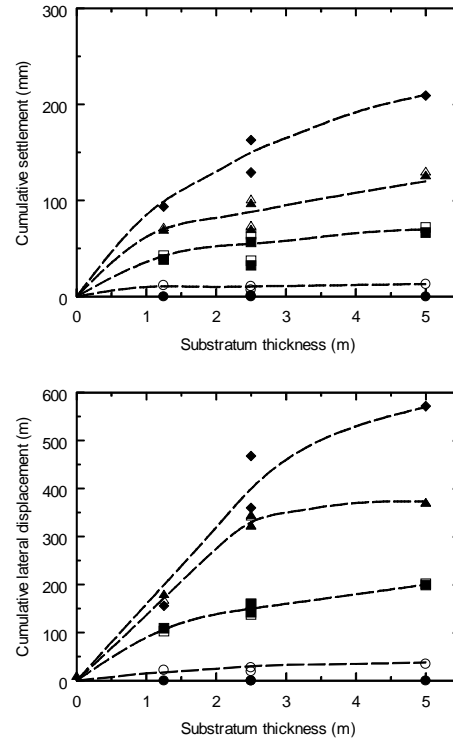


Figure 5. Effect of substratum thickness

Effect of Substratum Thickness

Figure 5 illustrates the effect of substratum thickness on displacement of the caisson, for tests where the relative density was approximately 55 %. Data from tests SW03, SW05, SW07, SW11 and SW12, where the thickness varied between 0 and 5 m, are shown. The data show that displacements do not increase in direct proportion to the substratum thickness (except perhaps for small thicknesses), with deformations for any given shaking event apparently trending towards an upper limit as the thickness increases. Increasing the substratum thickness from 1.25 to 5 m led to an increase in settlement by a factor of about two, and an increase in lateral displacement by a factor of two to three.

The relationship between thickness and displacement is likely to be influenced by the predominant period of the input motion and the natural period of the models with different layer thicknesses. This is possibly evident in the results shown in Figure 5, where the displacements during the Kobe events appear to show a slightly larger increase with increasing substratum thickness than the 3 Hz events. During the small strain events, the natural period of the models was observed to be between 0.15 and 0.25 s, lengthening with increasing substratum thickness. During the strong shaking events, the natural period lengthened to between about 0.5 and 1.2 s, lengthening with increasing shaking magnitude. The Kobe events caused a greater lengthening in period than the 3 Hz events. This point is discussed further by Stewart et al. (2000), who illustrate that unlike the 3 Hz event, the Kobe event contains significant energy content over a broad frequency range, encompassing the unsoftened (small strain) and softened (large strain) natural frequencies of the different models.

CYCLIC LOAD-DEFORMATION RESPONSE

In an attempt to understand the performance of the model in detail, an attempt was made to graphically relate the accelerations and displacements of the caisson, in a form similar to that commonly used to present the results of cyclic element tests conducted in the laboratory. The geometry of the model is complex and, despite the large number of instruments, there were insufficient data to derive the actual stresses and strains for one-dimensional conditions as described by Elgamal et al. (1996). Thus a number of parameters that would give approximate indicators of the stresses and strains were derived as follows:

- T^* \equiv Average dynamic shear stress at the surface of the sand substratum due to inertial loads imposed by accelerations of the caisson and mound. T^* was derived from the summation of the inertial loads of the caisson and mound divided by the contact area and does not include those forces applied by the backfill or armored embankment, or the initial static shear stress. Positive values of T^* correspond to stresses which induce straining away from the backfill.
- $\sigma'_{v,*}$ \equiv Estimate of the average vertical effective stress at the midpoint of the substratum layer. This quantity was derived from the estimated caisson and mound overburden, the vertical cyclic total stress induced by the vertical acceleration of the caisson, and the average pore pressure in the bottom sand layer beneath the caisson.
- S^* \equiv Normalized vertical displacement in the substratum below the caisson. S^* is defined as the mean vertical displacement of the caisson divided by the thickness of the substratum. S^* is analogous to vertical strain in an element test, but also includes vertical displacement induced by lateral squeezing (material transfer into or out of the region beneath the caisson) of the substratum. Negative values of S^* indicate settlement.
- H^* \equiv Normalized lateral displacement of the caisson. H^* is defined as the mean horizontal displacement of the caisson base divided by the thickness of the substratum, and is analogous to shear strain in an element test. Positive values of H^* correspond to straining away from the backfill.

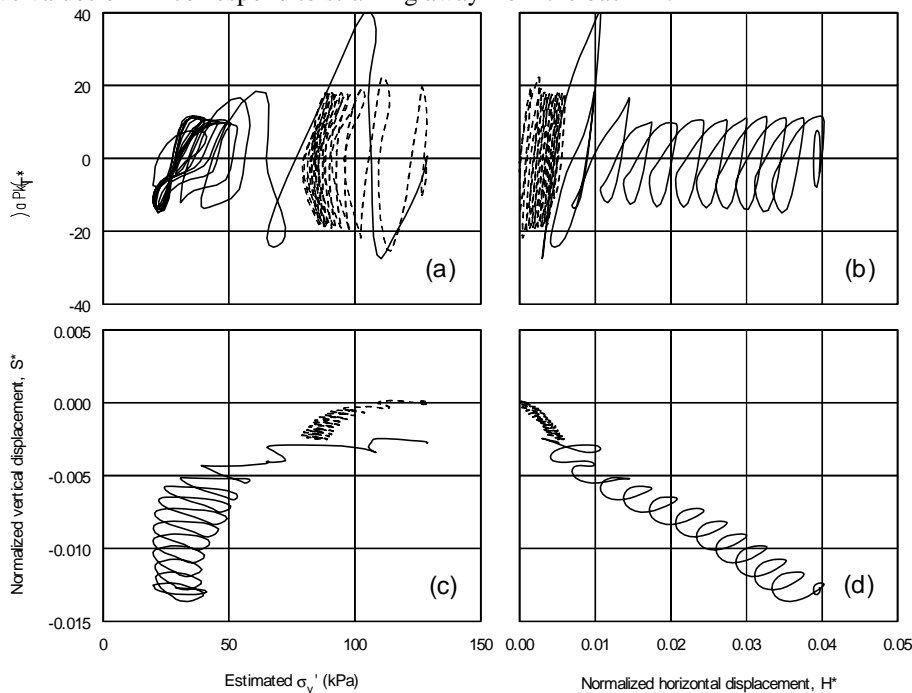


**Figure 6. Load-deformation response of caisson and substratum
0.1 g (dashed line) and 0.4 g (solid line) 3 Hz events.**

The evolution of these values during the 0.1 and 0.4 g 3 Hz events are presented in Figure 6, and results for the 0.6 g event are presented in Figure 7. In Figure 7, the final base driven cycle is shown with a thick solid line and arrows are included to indicate the direction of travel. Presentation of the data using these parameters combines the data from several instruments to provide illustration of the data which is more comprehensible than a series of time histories. The resulting data plots should be viewed as tools to observe the available data which, in this case, do not allow accurate calculation of actual stresses and strains. The $T^* - \sigma'_{v,*}$ (analogous to $\tau - \sigma'_v$) plots in

Figure 6(a) and 7(a) show strong similarity to the results of cyclic element tests on sand, where a cyclic shear stress is superimposed on a static shear stress (e.g. those illustrated by Mohamad and Dobry 1986 and Gu et al. 1993). In the 0.1 g event, the effective stress reduces gradually and cyclic shear deformations diminish with time. In the 0.6 g event, effective stresses drop near zero and cyclic dilatancy is apparent as σ'_{v*} increases and decreases with each cycle of T^* . The lack of symmetry in the cyclic paths is consistent with the presence of a static shear stress, and shear stress reversal.

The $T^* - H^*$ (analogous to $\tau - \gamma$) plots show initially relatively stiff response in the 0.1 g event, with little evidence of strain softening. However, in the larger events there is considerable residual strain developing as the event progresses, and a noticeable softening of the stress-strain curve. In the 0.6 g event, the concave upward $T^* - H^*$ curve is evidence of stiffening due to dilation at large strains in the later cycles. This occurs as a positive shear stress develops (movement away from the backfill), which correlates with the increase in σ'_{v*} in Figure 7(a). There is also some evidence of dilation (increasing σ'_{v*}) with movement in the opposite direction, in the 0.6 g event. The presence of a static shear stress on a contractive soil will reduce its cyclic resistance, and depending on the relative magnitudes of the static and cyclic stresses and the steady state strength of the soil, flow deformation may occur (Mohamad and Dobry, 1986). However, for partially contractive soils (within the transition region from contractive to dilative behavior, Alarcon-Guzman et al. 1988) the effect of a static shear stress depends on the strain level, with contractive behavior at small strains and dilative behavior at large strains. The derived load paths are consistent with partially contractive behavior.

The $S^* - \sigma'_{v*}$ (analogous to $\epsilon_v - p'$) plots show that settlement increases as σ'_{v*} decreases. The majority of the settlement occurs when the effective stress is low, again suggesting that the vertical movement may be largely caused by undrained lateral squeezing. However, the complexity of the model, and the available data, make it difficult to assess the true cause of the movement. The $S^* - H^*$ plots relate the development of vertical and lateral deformations. The value of S^* increases (upward movement) as the caisson moves away from the backfill (increasing H^*). These data indicate dilation of the soil when it is sheared in the direction away from the backfill. The dilation is largely suppressed when the soil is sheared towards the backfill, due to the static shear stress.

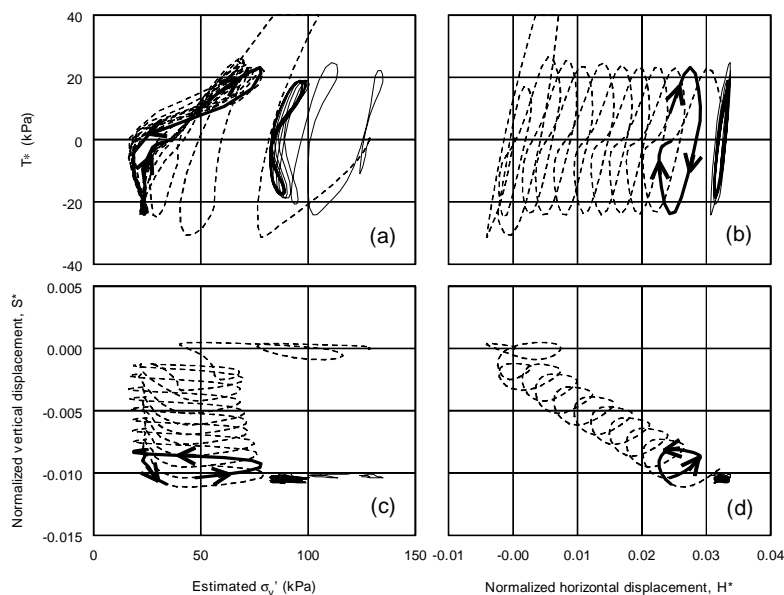


Figure 7. Load-deformation response of caisson and substratum 0.6 g (dashed and thick solid lines) and 0.1 g (thin solid line) 3 Hz events

Although not presented here, the same method of data presentation was applied to data from the Kobe event. Due to the more random nature of the input acceleration, the cyclic load-deformation response was less repetitive and more difficult to follow than for the sinusoidal base motions. However, the response was consistent with that described here, with several large load-deformation responses during large cycles of loading. The data presented in Figures 6 and 7 are consistent with expected soil behavior and show strong similarity to the results of laboratory element tests. Figures 6 and 7 represent data from 12 separate instruments. The encouraging results suggest that with sufficiently detailed instrumentation, the average stress-strain response of very complex models could be estimated with reasonable accuracy..

SUMMARY AND CONCLUSIONS

The performance of a model seawall structure, consisting of a caisson and armored embankment, has been studied using the large geotechnical centrifuge at the University of California, Davis. As expected, the caisson was found to settle, displace laterally, and rotate away from the backfill. However, the model deformations were relatively small when compared with the seawall failures observed in Kobe (which did not have armored embankments) during the 1995 Hyogo-Ken Nanbu earthquake. The largest observed deformations for the entire testing program was 0.21 m of settlement and 0.57 m of lateral displacement at the top of the caisson.

The seawall structure used in this study was subjected to a parametric study to determine the effects of substratum density, substratum thickness, partial substratum improvement, and backfill density. The settlement of the caisson is dependent on the soil density below the caisson, and the thickness of the substratum layer in this region. The settlements decreased with increased substratum density, and decreased substratum thickness. The lateral displacements of the caisson are mainly dependent on the soil layer density and thickness below the caisson and armored embankment. Due to the relatively detailed instrumentation of the models, an alternative method for plotting the data has been presented. The data from several instruments have been combined to allow easier visualization of the cyclic load deformation response within the substratum soils. The resulting load deformation curves bear strong similarity to stress paths in cyclic laboratory element tests.

This research has been supported by nine Japanese power companies and Japan Atomic Power Co. through the grant for Joint Research Program "Studies on development of siting technology of man-made island type NPP", 1995-1997.

REFERENCES

- 1) Alarcon-Guzman, A., Leonards, G. A., and Chameau, J. L. (1988) Undrained monotonic and cyclic strength of sands, *Journal of Geotechnical Engineering*, **114** (10), 1089-1109.
- 2) Elgamal, A.-W., Zeghal, M., Taboada, V. and Dobry, R. (1996) Analysis of site liquefaction and lateral spreading using centrifuge testing records, *Soils and Foundations*, **36** (2), 111-121.
- 3) Fiegel, G. L., Hudson, M., Idriss, I. M., Kutter, B. L. and Zeng, X. (1994) Effect of model containers on dynamic soil response, Proc. Int. Conf. Centrifuge 94, Singapore, Leung, Lee and Tan (ed's), Balkema, Rotterdam, 145-150.
- 4) Finn, W. D. L., Bransby, P. L., and Pickering, D. J. (1970) Effect of strain history on liquefaction of sand, *Journal of the Geotechnical Engineering Division, ASCE*, **96** (6), 1917-1933.
- 5) Gu, W. H., Morgenstern, N. R., and Robertson, P. K. (1993) Progressive failure of lower San Fernando dam, *Journal of Geotechnical Engineering*, **119** (2), 333-349.
- 6) Inagaki, H., Iai, S., Sugano, T., Yamazaki, H. and Inatomi, T. (1996) Performance of caisson type quay walls at Kobe port, *Soils and Foundations*, Special issue on geotechnical aspects of the January 17 1995 Hyogoken-Nambu Earthquake, 119-136.
- 7) Ishihara, K. and Okada, S. (1978) Effects of stress history on cyclic behavior of sands, *Soils and Foundations*, **18** (4), 31-45.
- 8) Kawai, T., Kanatani, M., Tanaka, Y., Stewart, D. P., Kutter, B. L., Settgast, R. R., Ishikawa, H., Takeda, T., Higuchi, S. and Goto, Y. (1998) Seismic performance of a caisson type seawall with an armored embankment, Proc. Int. Conf. Centrifuge 98, Kimura, Kusakabe and Takemura (eds), Tokyo, Balkema, Rotterdam, 351-358.
- 9) Kutter, B. L., Idriss, I. M., Kohnke, T. J., Lakeland, J., Li, X. S., Sluis, W., Zeng, X., Tauscher, R. C., Goto, Y. and Kubodera, Y. (1994) Design of a large earthquake simulator at UC Davis, Proc. Int. Conf. Centrifuge 94, Singapore, Leung, Lee and Tan (ed's), Balkema, Rotterdam, 169-175.
- 10) Mohamad, R. and Dobry, R. (1986) Undrained monotonic and cyclic triaxial strength of sand, *Journal of Geotechnical Engineering*, **112** (10), 941-958.
- 11) Schofield, A. N. (1980) Cambridge geotechnical centrifuge operations, *Geotechnique*, **30** (4), 227-268.
- 12) Seed, H. B., Mori, K., and Chan, C. K. (1977) Influence of seismic history on liquefaction of sands, *Journal of the Geotechnical Engineering Division, ASCE*, **103** (4), 257-270.
- 13) Stewart, D. P., Chen, Y. R. and Kutter, B. L. (1998) Experience with the use of methylcellulose as a viscous pore fluid in centrifuge models, *Geotechnical Testing Journal, GTJODJ*, **21** (4), December, ASTM, 365-369.
- 14) Stewart, D.P., Settgast, R.R., Kutter, B.L., Kawai, T., Higuchi, S., Ishikawa, H., and Takeda, T. (2000) Experimental performance of a seawall model under seismic conditions, submitted to *Soils and Foundations*.
Zeng, X. and Schofield, A. N. (1996) Design and performance of an equivalent-shear-beam container for earthquake centrifuge modelling, *Geotechnique*, **46** (1), 83-102.